Source distribution in interferometry for wave and diffusion

Yuanzhong Fan and Roel Snieder
Center for Wave Phenomena, Department of Geophysics, Colorado School of Mines, Golden, CO 80401

ABSTRACT
For the wave equation, the Green's function that describes the wave propagating between two receivers can be reconstructed by cross-correlation if the receivers are enclosed by sources on a closed surface. This technique is normally called interferometry. The ordinary operator used in this technique is cross-correlation. The same technique for Green's function extraction can be applied to the solution of the diffusion equation if there are sources throughout in the volume. In practice, we only have a finite number of active sources. We address the question what minimum source density is needed for the accurate extraction of the Green's function, and how these sources should be located on the source in the wave problem and if it is possible to reconstruct the Green's function of the diffusion equation by using a limited number of sources within a finite volume. We study these questions for homogeneous and isotropic media for both wave propagation and diffusion using numerical simulations. These simulations show that for the used model, the angular distribution of sources is critical in wave problems. For diffusion, the sensitivity of the sources decays away from the center of the two receivers. The required width of the source distribution decreases with frequency, and therefore the required source distribution for early time and late time reconstruction is different.

Key words: interferometry, waves, diffusion, virtual source

1 INTRODUCTION

The term interferometry generally refers to the study of the interference of two signals to obtain a measure of the difference between them (Curtis *et al.*, 2006). It also refers to the technique used to extract the response which describes the wave propagating between two receivers as if one of the receivers were an active source (Lobkis & Weaver, 2001; Derode *et al.*, 2003; Weaver & Lobkis, 2004; Wapenaar, 2004; Snieder, 2004; Snieder, 2007; Wapenaar *et al.*, 2005). This technique has also been applied in many fields: in ultrasound (Weaver & Lobkis, 2001; Malcolm *et al.*, 2004; van Wijk, 2006; Larose *et al.*, 2006), crustal seismology (Campillo & Paul, 2003; Shapiro *et al.*, 2005; Roux *et al.*, 2005; Sabra *et al.*, 2005a; Sabra *et al.*, 2005b), exploration seismology (Bakulin & Calvert, 2004; Calvert *et al.*, 2004; Bakulin & Calvert, 2006), helioseismology (Rickett & Claerbout, 1999), structural engineering (Snieder & Safak, 2006; Snieder *et al.*, 2006), and numerical modeling (van Manen *et al.*, 2005).

In seismic imaging, the studies of interferometry and its applications have grown rapidly in recent years. The seismic interferometry technique was first applied to wave propagation in non-attenuating and time-reversal invariance media (Lobkis & Weaver, 2001; Derode *et al.*, 2003; Weaver & Lobkis, 2004; Wapenaar, 2004; Snieder, 2004). Later, it was proved that Interferometry can not only be applied to wave fields, but also to diffusive fields (Snieder, 2006b). Recent proofs have been given that the Green's function can be extracted for a wide class of linear systems that may be attenuating, and that may not be invariant for time reversal because of flow (Godin, 2006; Wapenaar, 2006b; Wapenaar *et al.*, 2006; Snieder *et al.*, 2007; Weaver, 2008).

Seismic interferometry is in the exploration community referred to as the *virtual source method* (Bakulin & Calvert, 2004; Calvert *et al.*, 2004; Bakulin & Calvert,

2006), and has been applied to imaging (Mehta *et al.*, 2007a; Vasconcelos *et al.*, 2007). The sources used in this type interferometry can be either controlled shots (Bakulin & Calvert, 2004; Calvert *et al.*, 2004; Schuster *et al.*, 2004; Bakulin & Calvert, 2006; Mehta *et al.*, 2007a; van Wijk, 2006) or ambient noise (Weaver, 2005; Shapiro *et al.*, 2005; Roux *et al.*, 2005; Stehly *et al.*, 2006; Godin, 2006; Curtis *et al.*, 2006).

Although the extraction of the Green's function is usually based on cross-correlation, deconvolution can also be used (Snieder & Safak, 2006; Vasconcelos & Snieder, 2006). The term interferometry in this paper refers to the cross-correlation based interferometry.

Interferometry applied to fields governed by the wave equation can be expressed, in the frequency domain, as (Snieder *et al.*, 2007):

$$G(\mathbf{r}_A,\mathbf{r}_B,\omega) - G^*(\mathbf{r}_A,\mathbf{r}_B,\omega) = \oint_S \frac{1}{\rho}(G^*(\mathbf{r}_A,\mathbf{r},\omega)\nabla G(\mathbf{r}_B,\mathbf{r},\omega) - (\nabla G^*(\mathbf{r}_A,\mathbf{r},\omega))G(\mathbf{r}_B,\mathbf{r}))\widehat{n}dS, \quad (1)$$

where $G(\mathbf{r}_A,\mathbf{r}_B,\omega)$ is the displacement Green's function that describes wave propagation from receiver at $\mathbf{r}_B$ to the receiver at $\mathbf{r}_A$ respectively, $*$ indicates complex conjugation, $G(\mathbf{r}_A,\mathbf{r},\omega)$ and $G(\mathbf{r}_B,\mathbf{r},\omega)$ are the Green's functions that describe waves received by receiver A and B from a source at position $\mathbf{r}$, S is the surface where sources are located, $\widehat{\mathbf{n}}$ is the unit vector perpendicular to the surface dS, ω is the angular frequency, ρ is the density and c is the medium velocity. When the waves satisfy a radiation boundary condition on the surface S, $\nabla G(\mathbf{r}_A,\mathbf{r},\omega) \approx i(\omega/c)G(\mathbf{r}_A,\mathbf{r},\omega)\widehat{\mathbf{r}}$, and equation (1) becomes

$$G(\mathbf{r}_A,\mathbf{r}_B,\omega) - G^*(\mathbf{r}_A,\mathbf{r}_B,\omega) \approx \frac{2i\omega}{\rho c}\oint_S G(\mathbf{r}_A,\mathbf{r},\omega)G^*(\mathbf{r}_B,\mathbf{r},\omega)(\widehat{\mathbf{r}}\cdot\widehat{\mathbf{n}})dS, \quad (2)$$

In the time domain, equation (2) states that integrating the cross correlation of wave fields at receiver A and B from one source over the surface S and taking the time derivative of it, we obtain the response between the two receivers where one of them acts as a source. In addition to the causal response G, we also retrieve the time-reverse G^* of this response. Using the geometric relationship defined in figure 1, equation (2) becomes

$$G(\mathbf{r}_A,\mathbf{r}_B,\omega) - G^*(\mathbf{r}_A,\mathbf{r}_B,\omega) \approx \frac{2i\omega}{\rho c}\oint_{S'} G(\mathbf{r}_A,\mathbf{r},\omega)G^*(\mathbf{r}_B,\mathbf{r},\omega)dS', \quad (3)$$

in which $dS' = dScos\psi$ is the projection of the surface element dS on a circle with radius r.

The expression for Green's function extraction for fields governed by the diffusion equation is similar to that for waves. The main difference is that the surface integral becomes a volume integral (Snieder, 2006b):

$$G(\mathbf{r}_A,\mathbf{r}_B,\omega) - G^*(\mathbf{r}_A,\mathbf{r}_B,\omega) = 2i\omega\int_V G(\mathbf{r}_A,\mathbf{r},\omega)G^*(\mathbf{r}_B,\mathbf{r},\omega)dV, \quad (4)$$

in which V is the volume containing the sources. The meaning of other terms are the same as those in equation (3).

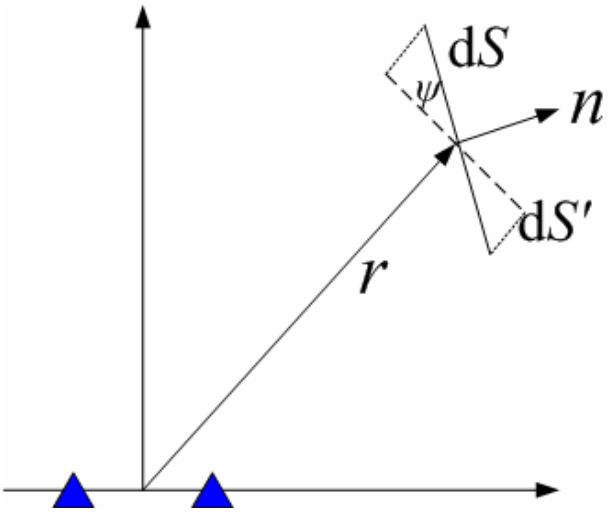

Figure 1. An arbitrary surface dS and its projection dS'

Equations (3) and (4) show that the main difference between wave and diffusion interferometry is the required source distribution. For waves, equation (3) shows that if two receivers are surrounded by active sources on a closed surface, the response which describes the wave propagating between the two receivers can be reconstructed as if one of the receivers were an active source. For diffusion, equation (4) states that the sources are required to be everywhere in the volume (Snieder, 2006b). In practice, there are only a finite number of sources. Therefore, we can never have a closed source surface for waves or sources throughout the volume for diffusion. This raises the question: what is the required source density and how should we locate these sources in order to reconstruct the Green's function accurately?

The importance of cross-correlation-based interferometry for waves has been addressed by numerous authors. On the other hand, cross-correlation-based interferometry for diffusion is still at the theory stage and there are no field applications yet. In exploration geophysics, there are at least two important diffusive fields: pore pressure and low-frequency inductive electromagnetic fields. From the pore pressure we can infer the fluid conductivity between wells (Voyiadjis & Song, 2003; Nokken & Hooton, 2007). Electromagnetic fields carry information about the resistivity of the pore fluid and may thus help distinguish between hydrocarbons and water. For the offshore oil exploration, controlled-

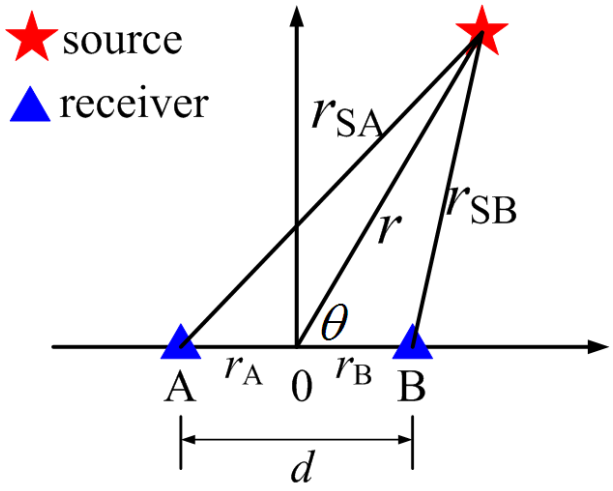

Figure 2. Definition of the source radius r and source angle θ that define a source position in 2-D.

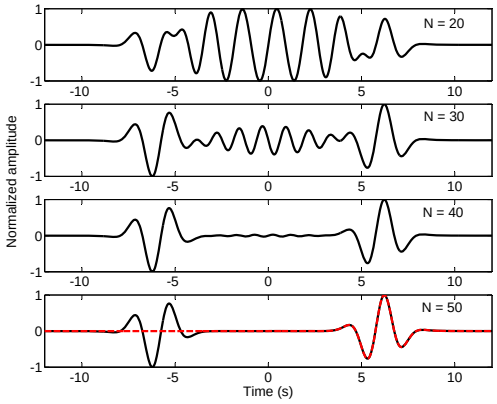

Figure 3. Reconstructed responses (solid lines) for uniform angle distribution with different number of source N (the dashed line in the bottom panel is the exact response between the two receivers)

source electromagnetic (CSEM) is one of the most important techniques used to detect hydrocarbon (Hoversten *et al.*, 2006; Constable & Srnka, 2007; Darnet *et al.*, 2007; Scholl & Edwards, 2007).

In this paper, we study the required source distribution in a simple homogeneous model for both waves and diffusion with a finite number of sources.

MODEL AND RESULTS

Waves

For simplicity, we first use a 2-D homogeneous model, with constant velocity 1 km/s, in the numerical tests. For defining the source position, we use two parameters: source angle and source radius as shown in Figure 2. A and B are two receivers with a separation d. The position vectors of the two receivers are denoted by $\mathbf{r}_{SA}$ and $\mathbf{r}_{SB}$, respectively. The source function for waves we use in all the examples in this paper is a Ricker wavelet with a central frequency of 0.5 Hz. The source amplitude is the same for all sources.

Experiment 1: uniformly distributed source angle.

We first study the effect of the source angle distribution. Sources are uniformly distributed on the circle with a radius of 40 km. The distance between the two receivers is 6 km. Figure 3 shows the reconstructed response between the two receivers for a homogeneous distribution of sources with increasing source number. The response has two parts, the causal and anti-causal parts as represented by equation (3). The causal part of the signal represents the signal propagating from receiver A to B and the anti-causal part is the time-reverse of this, i.e. the signal propagating from receiver B to A. If we replace one of the receivers with an active source, the received signal arrives after a propergation time of 6 s. To make the shape of the received signal the same as the reconstructed signal, we correlate the received signal with the source-time function. This new signal is represented by the dashed line in the bottom panel, it is virtually the same as the causal part of the reconstructed response with 50 sources (the amplitudes of both reconstructed and active signals are normalized). The main point in figure 3 is that the fluctuation energy in the middle part of the reconstructed signal decreases with increasing source number N, and a minimum source density needs to be exceeded in order to extract the response successfully. This required source density is derived in the discussion part of this section.

We quantify the spurious fluctuations that arrive between the anti-causal and the causal response by defining the fluctuation energy

$$E_m = \frac{1}{N_m} \sum_{i=1}^{N_m} A[i]^2, \tag{5}$$

in which N_m is the number of discrete sample points in the middle part of the signal, i.e. the part between the two main pulses. Figure 4 shows this fluctuation energy decay as a function of source number N. Weaver and Lobkis (Weaver & Lobkis, 2005) showed that these fluctuations decay as N^{-1} if the sources are randomly distributed . Figure 4 shows that when the sources are uniformly distributed in angle, the decay rate is much faster than N^{-1}. The reason of this is shown in the disscusion part of the wave problem.

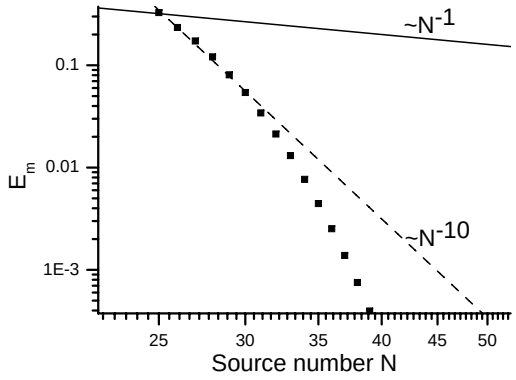

Figure 4. Fluctuation energy decay as a function of source number N for the uniform angle distribution. The dashed and solid line represent two different power-laws in the log-log coordinate system.

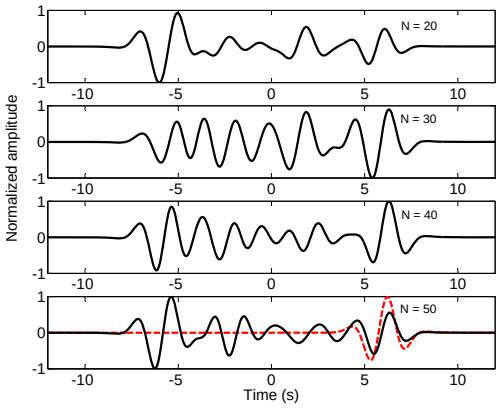

Figure 5. Reconstructed responses (solid lines) for random angle distribution with different number of sources N (the dashed line in the bottom panel is the exact response between the two receivers).

Experiment 2: randomly distributed source angle.

In this experiment, the source angles are randomly distributed while the source radius is constant. Figure 5 shows the reconstructed response as a function of source number N for a random distribution of sources along the circle. Compared with figure 3, the random distribution gives a much poorer reconstruction than does the uniform distribution with the same source number.

Figure 6 shows this fluctuation energy decay, as defined in equation (5), as a function of N for randomly distributed sources. The fluctuation decay behavior is consistent with the prediction of Weaver and Lobkis(2005): the decay is proportional to N^{-1}. Experiment 2 suggests that not only the number of the source is important, but also their angular distribution. The difference of this decay rate of uniformly and randomly distributed sources is explained in the discussion part of this section.

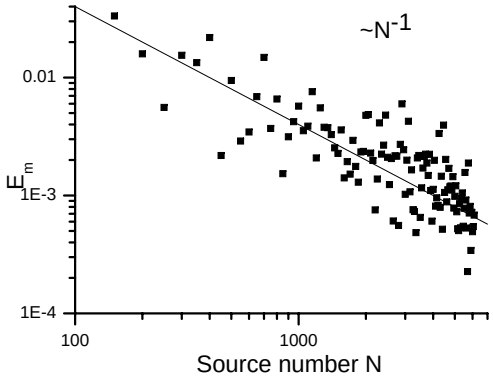

Figure 6. Fluctuation energy decay as a function of source number N for the random angle distribution. The solid line represents a N^{-1} power-law decay in the log-log coordinate system.

Experiment 3: smooth source angle distribution.

From experiments 1 and 2, we might conclude that the source angle needs to be uniformly distributed to apply this technique successfully with a small number of sources. This experiment shows that the angle is not necessary to be uniformly distributed but is smoothly varying. Next we show examples with non-uniform but smoothly varying angle distribution where the response is accurately reconstructed.

In the example shown in figure 7, sources are uniformly distributed on the circle with the center of the two receivers moved away from the center of the circle (from (0,0) to (-5,6)). This makes the source angle distribution no longer uniform, but it's still smooth. The numerical simulation shows accurate reconstruction of the response from 50 sources. The amplitude difference of the causal and anti-causal parts are due to the different energy from the two stationary-phase zones on the left and right side of the receivers as illustrated by the two dashed curves in the upper panel of figure 7. Only the sources within these two stationary zones contribute to the extraction of the direct wave (Snieder, 2004; Roux *et al.*, 2005). In this case, the stationary zone on the right side corresponds to the causal pulse and the left stationary zone corresponds to the anti-causal pulse. We notice that in the right stationary zone there are more sources than on the left side. This explains why the causal pulse is stronger than the anti-causal one. Notice that the distance of the sources to the midpoint of the receiver locations is not constant in this experi-

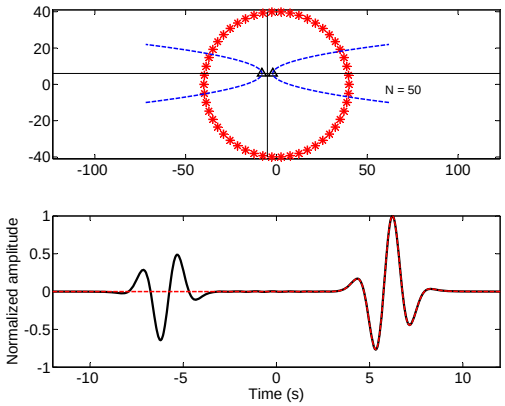

Figure 7. Reconstructed response (solid line in the lower panel, dashed line is the exact reponse) for a smoothly varying source angle distribution (upper panel)

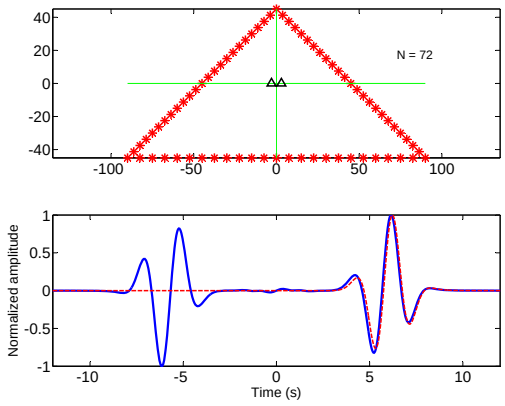

Figure 8. Reconstructed response (solid line in the lower panel, dashed line is the exact reponse) for source spaced equidistantly on a triangle (upper panel)

ment. One might think that the geometrical spreading also affects the amplitude of the reconstructed signal.

In the example shown in figure 8, sources are uniformly distributed on the sides of a triangle. The source angle is not uniform but smoothly varying. The lower panel in figure 8 shows that for the employed number of sources, the reconstruction of the response is still accurate. In this case, the required source number is a little bit larger than that for the uniform distribution but much smaller than for the accurate reconstruction of the Green's function with the random source distribution. The value of this number depends how smooth the angle is varying. This geometry is closer to the practical cases in which controlled sources are distributed on a line (Bakulin & Calvert, 2006; Mehta *et al.*, 2007a).

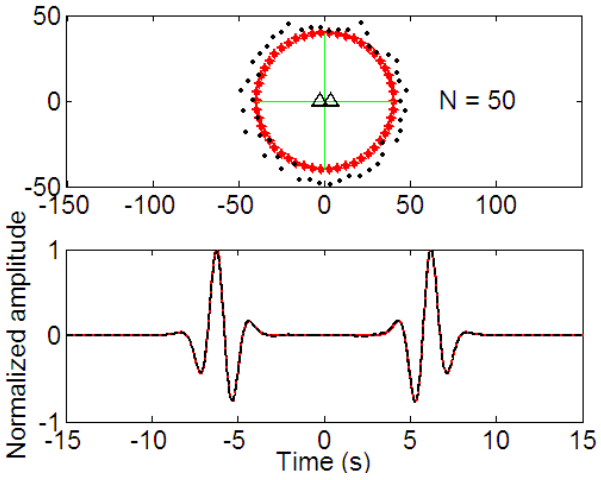

Figure 9. Two source distributions with the same angle distribution but different radii (top) and the reconstructed responses: red solid (same radius), black dashed line (different radius)

Note that in this example the source radii are much larger than the distance between the two receivers. In this case, the influence of varying source radii is negligible. This is shown in detail in the next experiment.

Experiment 4: source radius importance.

In the previous three experiments we learned how the angle distribution influences the response extraction. The best angle distribution is the uniform distribution and the decay rate of the non-physical fluctuations in the middle part is faster than N^{-10}. The slowest fluctuation decay is from the random angle distribution: and varies with the number of sources as N^{-1}. The number of source required for a smoothly varying angle distribution is close to the uniform distribution and the value of the number depends on how smooth the angular distribution is. There is, however, still another parameter: the radius r as defined in figure 2. In the next example we compare the result from two distributions with the same angle distribution but different source radii. The first one is the example we showed in experiment 1, when 50 sources are uniformly distributed on a circle (stars in the upper panel of figure 9). The second one is for sources with the same angle distribution but the radius is randomly varying in a range in which all radii are much larger than the distance between the two receivers (dots in the upper panel of figure 9. The reconstructed responses in figure 9 suggest that varying the source radii does not degrade the accuracy of the Green's function extraction. This is only true when source radii are much larger than the distance between the two receivers. The reason for this is explained in the discussion part.

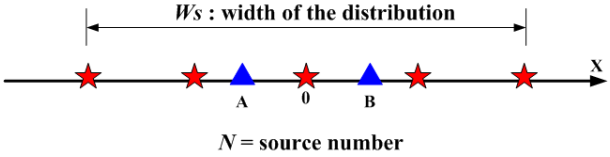

Figure 10. 1-D source distribution and the definitions of geometric parameters.

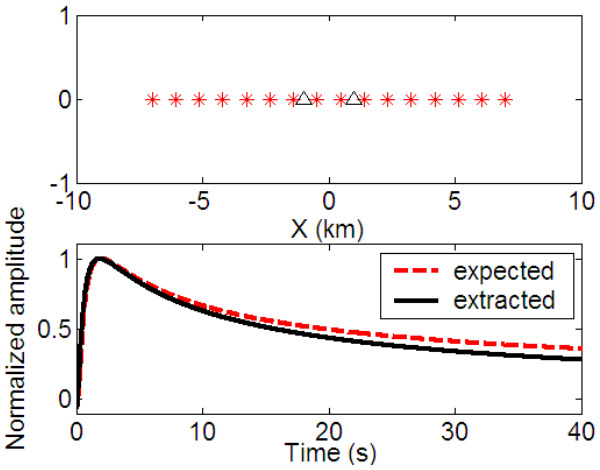

Figure 11. 1-D source distribution (upper panel) with Ws=14 km, ρ_s=1.143 km^{-1} and the extracted Green's function (lower panel).

Diffusion

Equation (4) shows that sources in the whole volume are needed to extract the Green's function for diffusion. To simplify the problem, we start with a 1-D medium with constant diffusion coefficient. Then we extend this to 3-D.

Experiment 1: diffusion Green's function recovery in 1-D.

We choose the origin of the coordinate system at the center of the two receivers. The distance between the two receivers is 2 km. The diffusion coefficient used in this model is $D = 1\ km^2/s$. We distribute sources uniformly on the 1-D line with the center of the distribution at origin. Figure 10 shows the geometry of 1-D source distribution.

We define two parameters to characterize this source distribution. As shown in figure 10, Ws is the width of the distribution and $\rho_s = N/Ws$ is the source density. Next we test three different distributions. The first one is a distribution with narrow width Ws and high source density ρ_s (figure 11). The second one is a distribution with the same number of sources, but with a wide width Ws and low density (figure 12). The third distribution has more sources and has wide Ws and high density ρ_s (figure 13).

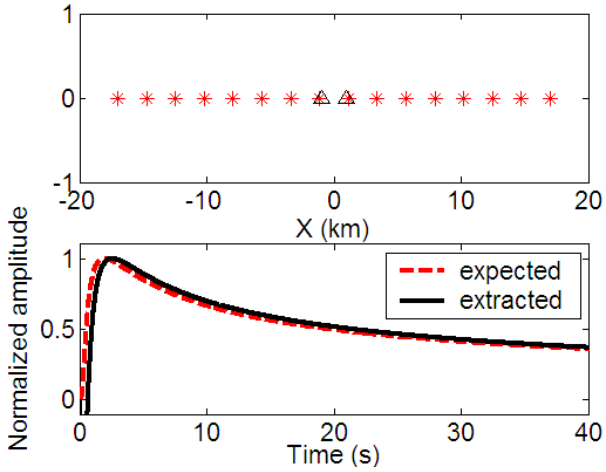

Figure 12. 1-D source distribution (upper panel) with Ws = 34 km, ρ_s = 0.47 km^{-1} and the extracted Green's function (lower panel).

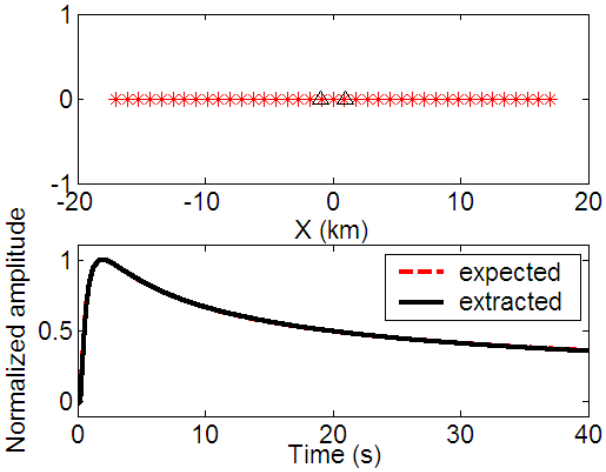

Figure 13. 1-D source distribution (upper panel) with Ws = 34 km, ρ_s = 1.147 km^{-1} and the extracted Green's function (lower panel).

Figures 11 to 13, show that for the reconstruction of the Green's function, different source distributions are needed for the accurate reconstruction of the early-time and the late-time response. The early time response is defined as the response before the peak in the Green's function of the diffusion equation, the late time part is defined as the response after the main peak. The early-time reconstruction is controlled by the source density ρ_s (figure 11 and 13) and late-time reconstruction is more affected by the distribution width Ws (figure 12 and 13).

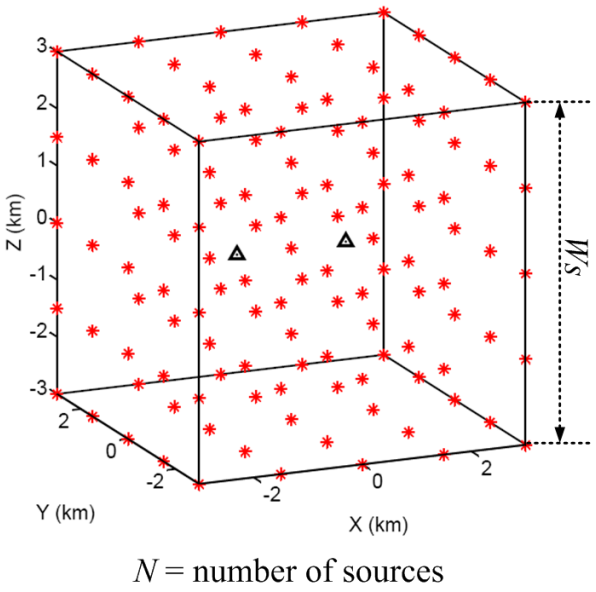

Figure 14. 3-D source distribution for diffusion interferometry.

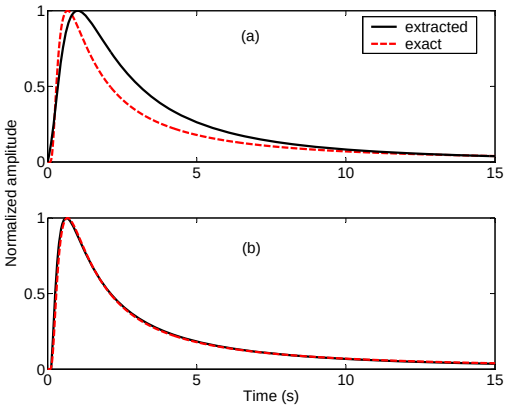

Figure 15. 3-D reconstruction of diffusion Green's function. (a) $Ws = 2.5$ km and $\rho_s = 0.51\ km^{-3}$. (b) $Ws = 10$ km and $\rho_s = 0.51\ km^{-3}$.

Experiment 2: Green's function recover for diffusion in 3-D.

Following the same strategy we extend the diffusion experiment to 3-D. Instead of putting the sources on a line, we uniformly distributed them in a cube as shown in figure 14. We define Ws as the side length of the cube, and the source density is defined as $\rho_s = N/(Ws)^3$.

In figure 15a, a source distribution with small Ws is used. As in 1-D, the early-time of the Green's function is reconstructed well, but the late-time behavior is not. When the width of the distribution increased, with sufficiently high source density ρ_s, both early and late time can be extracted well (figure 15b). In the 3 -D diffusion problem, higher source density is not always helpful for an accurate reconstruction. When the sources are getting too close to the receiver position, the drawback of the spatial singularity becomes severe. Consequently, the reconstruction is less accurate.

DISCUSSION

Waves in homogeneous media

The Green's function of the wave equation in 2D is represented in the frequency domain by the first Hankel function of degree zero (Snieder, 2006a):

$$G(r) = \frac{i}{4} H_0^{(1)}(kr). \tag{6}$$

In all the numerical simulations in this paper, we use the far field approximation of equation (6), which is

$$G(r) = \sqrt{\frac{1}{8\pi kr}} e^{i(kr+\pi/4)}. \tag{7}$$

Inserting this into equation (3), we obtain

$$G(\mathbf{r}_A, \mathbf{r}_B, \omega) - G^*(\mathbf{r}_A, \mathbf{r}_B, \omega) \approx \frac{i}{4\pi\rho} \oint_{S'} \sqrt{\frac{1}{r_{SA} r_{SB}}} e^{ik(r_{SA}-r_{SB})} dS', \tag{8}$$

When the source radius is much larger than the distance between the two receivers, the distance in the geometrical spreading can be approximated as $r_{SA} \approx r_{SB} \approx r$, while for the phase the approximation $r_{SA} - r_{SB} \approx dcos\theta$ is accurate to first order in d/r. (These parameters are defined in figure 2.) Using these approximations and the relationship $dS' = rd\theta$, equation (8) becomes

$$G(\mathbf{r}_A, \mathbf{r}_B, \omega) - G^*(\mathbf{r}_A, \mathbf{r}_B, \omega) \approx \frac{i}{4\pi\rho} \int_0^{2\pi} e^{ikdcos\theta} d\theta \tag{9}$$

Note that the right hand side does not depend on the source radius r. Experiment 4 in the wave part supports this conclusion: in that experiment, variations in the source radius do not influence the Green's function extraction.

The source radius enters this interferometry problem in three ways. The first one is the geometrical spreading term $1/r$, the second one is the relation between the surface element and the increment in source angle $dS' = rd\theta$, and the third one is the width of the stationary-phase zones as illustrated in the upper panel of figure 7. Equation (9) confirms that the first two factors compensate each other. Consequently, only the width of the stationary-phase zones contribute to the amplitude of the reconstructed signal. The different source number in the left and right stationary-phase

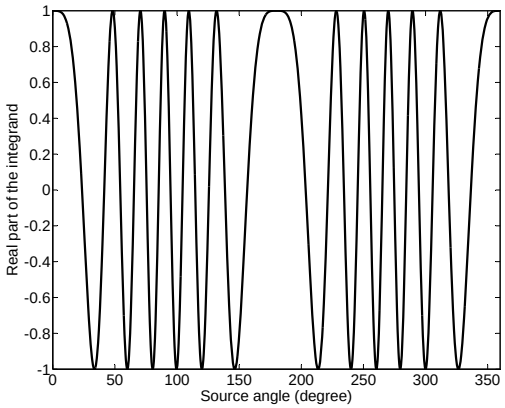

Figure 16. The real part of the integrand in equation (9).

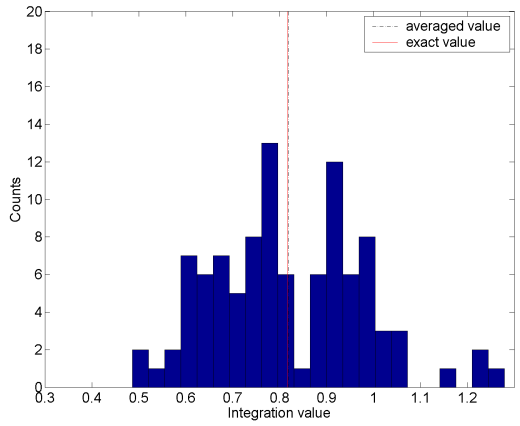

Figure 17. Histogram of 100 repeated estimations of the integral in figure 16.

zones cause the asymmetry in the amplitude of causal and anti-causal response as shown in the lower panel of figure 7.

Another interesting observation is that the right hand side of equation (9) is the integral representation of the Bessel function (Snieder, 2006a), which is related to the exact Green's function:

$$\frac{1}{2\pi}\int_0^{2\pi} e^{ikdcos\theta}d\theta = J_0(kd) = \frac{1}{2}(H_0^{(1)}(kd) - H_0^{(1)}(-kd)) \qquad (10)$$

This shows that by using only far field of the waves in the interferometry, both far field and near field response are reconstructed. This was shown for elastic waves by (Sánchez-Sesma *et al.*, 2006; Sánchez-Sesma & Campillo, 2006).

For the dependence on the angle θ, we need to study the character of the integrand in equation (9). The real part of this integrand is the oscillatory function shown in figure 16. The extraction of the Green's function depends on the sampling of this integral over source angle θ, and reduces to the numerical integration of a continuous oscillatory function. In the experiment we sum over all the sources to represent this integral. This actually assumes that the sampling in θ is uniform. Therefore if the sources are uniformly sampled in angle, this integral can be represented well by summation. Provided the sampling is sufficiently dense, with the random distribution of source angles, the angle separations are different everywhere. This would not give an accurate estimation of the integral just using summation. If the angle separation for each source is known, we can use this $d\theta$ as a weight in the summation as it does in the numerical integral. But if there is no information on $d\theta$, the average over repeated experiments would converge to the accurate reconstruction. Figure 17 shows a histogram of 100 repeated estimations of the integration of the function that is shown in figure 16. Each time, 1000 randomly distributed sources are used to estimate this integral. The estimation value at a specific realization can be far from the exact value while the average over all realizations (dashed line) is close to the accurate value (solid line). For the smoothly varying source angle, $d\theta$ is still fairly constant locally. Therefore oscillations cancel and the result is still accurate. For most of the applications of interferometry using control-shots, the source angle is actually smoothly changing (Bakulin & Calvert, 2006; Mehta *et al.*, 2007a). Here we explain why those smooth source angle distributions from experiment 3 for waves give accurate Green's function reconstruction.

Waves in heterogeneous media

We next investigate whether these observations for source distribution from a homogeneous medium also hold in heterogeneous media. To answer this question, we need to consider which parts of the problem are changing from a homogeneous medium to a heterogeneous one. Equation (3) is valid for any medium, regardless of its complexity. Therefore, we can still study the integrand in equation (3) as we show for the homogeneous case. For a homogeneous medium, this integrand becomes a simple form as shown in equation (9). For a heterogeneous medium the integrand can be in a very complicated form for the heterogeneous media. But the point is that we are still estimating the integral of this complicated function using summation. Consequently, the uniform angle distribution should still give the most accurate estimation. In order to support this statement, we show a comparison of two source distributions in a heterogeneous medium with 200 isotropic point scatters around the two receivers in figure 18. The wavefield was modeled using the theory of (Groenenboom & Snieder, 1995) that takes all multiple scattering events into ac-

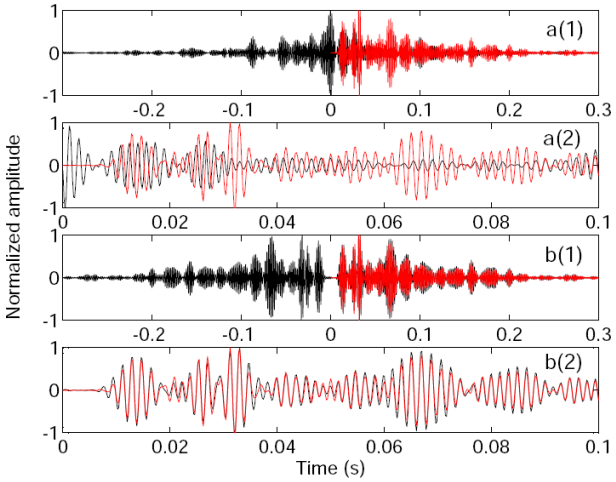

Figure 18. The Green's function reconstruction using a uniform and random distribution. The letter *a* denotes the case when 300 randomly distributed sources are used while *b* shows the case when 300 uniformly distributed sources are used. (1) and (2) show the same comparison in different scales.

count. In this theory the total wave field is written in summation of the primary field and the scattered field as

$$\psi(\mathbf{r}_i) = \psi_0(\mathbf{r}_i) + \sum_{j=1;j\neq i}^{n} G^{(0)}(\mathbf{r}_i, \mathbf{r}_j) A_j \psi(\mathbf{r}_j), \tag{11}$$

in which ψ_0 denotes the primary field, $G^{(0)}(r_i, r_j)$ is the Green's function between the scatter points $\mathbf{r}_j$ and $\mathbf{r}_i$, A_j is the scattering amplitude of scatterer j, and $\psi(\mathbf{r}_j)$ is the field incident on that scatterer. Then the system of linear equations are solved to calculate the total wave field. In figure 18, the red curve is the signal received by one receiver when the other one becomes a real source. The black curve is the signal reconstructed by interferometry. The letter *a* denotes the case when 300 randomly distributed sources are used while *b* shows the case when 300 uniformly distributed sources are used. (1) and (2) show the same comparison in different scales. The correlation coefficient between the exact and the causal part of the extracted signal is 0.97 for the uniform source distribution while it is -0.03 for the random distribution.

Note in some cases, the source distribution becomes less important. Malcolm (2004) showed that the ensemble averaged Green's function in a rock can be retrieved from a single source by moving the receiver pair around the source with uniform angle step. For a layered model with enough horizontal layers to give strong scattering, the full Green's function can be reconstructed by one-sided illumination with sources uniformly distributed on the free surface (Wapenaar, 2006a).

What is the minimum required source density if the sources are uniformly distributed in a homogeneous medium? As shown in figure 16, the oscillations have a variable period. In order to make the highest frequency oscillations cancel we need to have enough sampling points for the highest frequency. This oscillation depends on the phase term $\Phi = kdcos\theta$ of equation (9). The change in the phase for an angular increment $\Delta\theta$ is $\Delta\Phi = kdsin\theta\Delta\theta$. The most rapid oscillation happens at $sin\theta = 1$. In order to have N_r number of sources within the period of the most rapid oscillation, the required source density becomes

$$\rho_{source} = \frac{N_r kd}{2\pi}\ (radian^{-1}), \tag{12}$$

From experience, when $N_r > 2.5$, the fluctuation energy between the two main pulses in the reconstruction vanishes, this gives the sampling criterion

$$\rho_{source} = 0.4kd\ (radian^{-1}), \tag{13}$$

In conclusion, for wave interferometry in a homogeneous model, the most important parameter is the source angle distribution. If we know the source distribution, and hence the source angle, different weight function can be used to estimate the oscillation function better. If randomly distributed sources are used and there is no information on the source angle distribution, the average over large amount of extracted signals is more accurate to describe the real response. Otherwise, we need to choose the source angle smoothly varying to apply this technique accurately.

This conclusion holds when all sources have the same amplitude. If the amplitude of the sources fluctuates randomly, a uniform angle distribution gives similar reconstruction of the Green's function as the random angle distribution for a constant source strength. For a heterogeneous medium, the importance of the source distribution depends on how strong the heterogeneities are.

Diffusion

The frequency domain Green's function of the diffusion equation in a 1-D homogeneous medium is given by

$$G^{1D}(x,\omega) = \frac{1}{(1+i)\sqrt{2\omega D}} e^{(-1-i)x\sqrt{\omega/2D}} \tag{14}$$

Inserting this expression into equation (4), gives

$$G(\mathbf{r}_A, \mathbf{r}_B, \omega) - G^*(\mathbf{r}_A, \mathbf{r}_B, \omega) = \frac{i}{2D} \int_x e^{-(r_{SA}+r_{SB})\sqrt{\omega/2D}} e^{-i(r_{SA}-r_{SB})\sqrt{\omega/2D}} dx \tag{15}$$

Similar as for the analysis of the wave, we study the real part of the integrand of equation (15) as a function of space variable x. Notice that the integrand is also a function of frequency ω. Therefore, for different frequencies the real part of the integrand behaves differently. Figure 19 shows this integrand for two different frequencies. The width of the distribution decreases with fre-

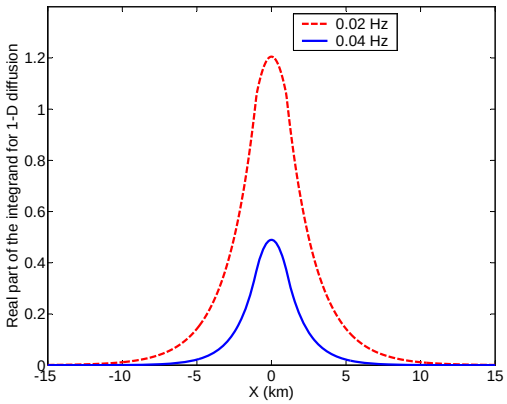

Figure 19. The real part of the integrand in equation (15) at two different frequencies.

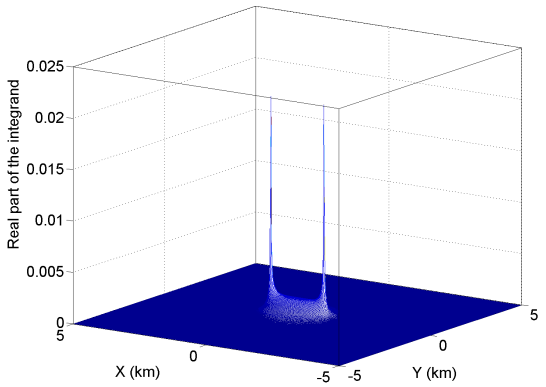

Figure 20. The real part of the integrand in equation (17) at frequency 0.15 Hz.

quency. Quantitively we can conclude that because the early time behavior of the Green's function has more high frequency components, the required source distribution can be narrower. This explains experiment 1 of the diffusion part: with small Ws, the early time behavior is reconstructed well. With increasing Ws, more lower frequency components are recovered. Since the tail of the Green's function mostly contains low frequencies, Green's function of late time is recovered accurately with a large width Ws. Consequently, the source density ρ_s controls the retrieval of the high frequency components of the Green's function (eg. early time of the Green's function), and the width of the distribution Ws controls lower frequency components (e.g. the late time of the Green's function).

The frequency domain Green's function for diffusion in 3-D is

$$G^{3D}(r,\omega) = \frac{1}{4\pi D r} e^{(-1-i)r\sqrt{\omega/2D}} \tag{16}$$

Inserting this into equation (4) we obtain

$$\begin{aligned} G(\mathbf{r}_A,\mathbf{r}_B,\omega) - G^*(\mathbf{r}_A,\mathbf{r}_B,\omega) = \\ 2i\omega \int_V \frac{1}{(4\pi D)^2 r_{SA} r_{SB}} e^{-(r_{SA}+r_{SB})\sqrt{\omega/2D}} \\ e^{-i(r_{SA}-r_{SB})\sqrt{\omega/2D}} dV \end{aligned} \tag{17}$$

The real part of the integrand is not easily displayed as a function of three volume variables. Since it is invariant for rotation along the axis joining the receivers(the x-axis in the used coordinate system), we display its behavior in the x-y plane. Figure 20 shows the real part of the integrand of equation (17) at a frequency of 0.15 Hz. There are two isolated peaks at the location of the two receivers. These peaks at the locations of the two receivers correspond to the two singularities in equation (17). It seems that the largest contribution to the integral comes from the sources at the positions of the receivers. These singularities are, however, integrable. In the numerical integration, if there are no sampling points at the singularities, the integration is still accurate as in the example of figure 15. In contrast, if there are sources very close the singularities, the integration is inaccurate because of the contributions from the singularities. But if there is a source very close to one of the receivers, there in no need for the interferometric extraction of the Green's function because this function can then be directly recorded by the other receiver.

This explains that why we can reconstruct the 3-D Green's function for diffusion in the experiment 2 of the diffusion part even though there are two singularities in equation (17). Because of these singularities, we should not have any sampling point very close to or at the singularities when we do numerical simulations or reality. This suggests that high source density in 3-D diffusion problem does not always give accurate Green's function extraction since some sources might be too close to the singularities.

We next address the question how to quantify the required source distribution width Ws and source density ρ_s. As we learned from the examples in the diffusion part, Ws determines the late time reconstruction of the Green's function. Suppose that the diffusion Green's function needs to be reconstructed accurately up to time τ_a (as shown in figure 21a), sources contribute up to a source-receiver distance: $r^2_{max}/(4D\tau_a) = 1$. This is based on the decay term $e^{-r^2/(4Dt)}$ in the time domain Green's function of diffusion equation. Therefore, the required Ws should be

$$Ws = 4\sqrt{D\tau_a} + d \tag{18}$$

for an accurate reconstruction up to time τ_a, in which d is the distance between the two receivers. Figure 21b shows the error of the reconstruction at τ_a and $2\tau_a$ by using different Ws. The error is defined as the ratio of

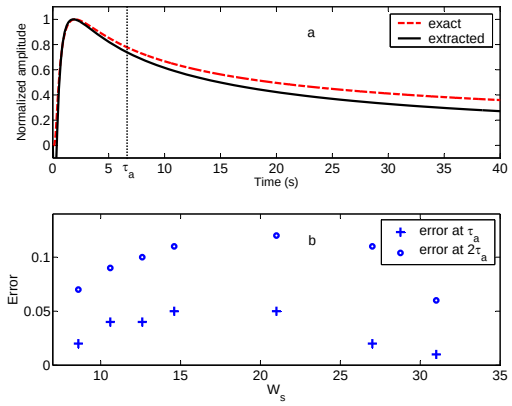

Figure 21. The upper panel is the definition of tau_a up to which the Green's function would be estimated accuratly. The lower panel shows the error in the reconstructed Green's function at time tau_a and $2tau_a$ by using source width Ws defined from equation (18).

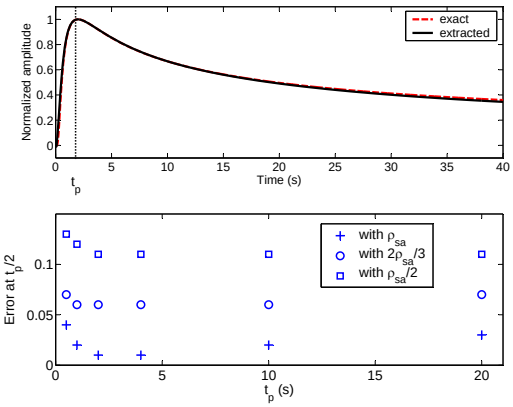

Figure 22. The upper panel is the definition of peak time in the Green's function. The lower panel shows the error at $t_p/2$in the reconstructed Green's function for varying peak time t_p using different source density. rho_{sa} is defined in the equation (21).

the difference between the exact and extracted signals to the exact signal. The time τ_a for a certain Ws is determined by equation (18). The model parameters used in this test are the same as those in the experiment 1 of the diffusion part. For this sampling criterion, the error in the Green's function up to τ_a is less than 5%.

The other parameter ρ_s controls the early time reconstruction. In other words, it determines the accuracy of the reconstruction for the high frequency components. For the maximum frequency f_m in the problem – either the highest frequency component of the Green's function itself or the maximum frequency of the source function – there is a sensitivity function of source position as shown in figure 19 for the 1-D problem or figure 20 for the 3-D problem. This sensitivity is controlled by the decay factor is $e^{-(r_{SA}+r_{SB})\sqrt{\omega/2D}}$ as shown in equation (15) and (17). The $1/e$ width of this sensitivity function is:

$$\sigma = \sqrt{2D/\omega} \tag{19}$$

Then if N_r is the number of source needed in this range σ to estimate the integral accurately, the required source density is:

$$\rho_{sa} = N_r\sqrt{\omega/2D} \tag{20}$$

Based on the numerical examples, when N_r is larger than 2, it is adequate to reconstruction the early time response. Then equation (20) becomes:

$$\rho_{sa} = 2\sqrt{\omega/2D} \tag{21}$$

We can estimate the maximum frequency component in the Green's function as $1/(4t_p)$,in which t_p is the arrival time of the amplitude peak in the Green's function. Figure 22 shows the error in the reconstructed Green's function at time $t_p/2$ using different source densities. Green's functions with different t_p are tested. The adequate source density ρ_{sa} is calculated using equation (21).

In conclusion, for cross-correlation-based diffusion interferometry, instead of having sources everywhere in the volume, it suffices to have sources in only a small volume surrounding the receivers as shown in figures 19 and 20. For the 1-D problem, the source distribution width controls the late-time (low-frequency components) reconstruction of the Green's function and source density controls the early-time (high-frequency components) reconstruction. For the 3-D problem, sources should not be located too close to the receivers position because of the singularities. As we focus on the possibility of diffusion Green's function reconstruction and the uniform source distribution is the best case to understand this problem, we do not include non-uniform source distribution in this paper.

Let us consider next what happens if we apply deconvolution rather than cross-correlation. For the 3-D Green's function of the diffusion in equation (16), the deconvolution of G_A and G_B is given by

$$\frac{G_A}{G_B} = \frac{r_{SB}}{r_{SA}} e^{(-1-i)(r_{SA}-r_{SB})\sqrt{\omega/2D}} \tag{22}$$

So if we have a single source on the x axis and outside of the two receivers, equation (22) becomes

$$\frac{G_A}{G_B} = \frac{r_{SB}}{r_{SA}} e^{(-1-i)d\sqrt{\omega/2D}} = \frac{r_{SA}}{4\pi D d r_{SB}} G_{AB} \tag{23}$$

From this equation we can see that, apart from a scaling factor, deconvolution gives us an accurate reconstruction for a single source. This shows that cross correlation and deconvolution behave different for diffusion

problem. Deconvolution-based interferometry might be a better approach to diffusion problem, but this may be a peculiarity of the homogeneous medium. For waves, researchers have started to use deconvolution-based interferometry (Trampert *et al.*, 1993; Snieder & Safak, 2006; Vasconcelos & Snieder, 2006; Mehta *et al.*, 2007b).

Conclusion

The cross-correlation-based interferometry used to extract the Green's function which describes the field propergation between two receivers can be applied to the solution of both the wave equation and the diffusion equation. The main difference is the required source distribution.

For interferometry for the wave equation in a homogeneous medium, the source angle distribution is the most important parameter. With the assumption that the source radii are much larger than the distance between the two receivers, the variation in the source radius has a negligible effect and the interferometry problem can be represented by a numerical integral of an oscillatory function of source angle. If cross-correlations from different sources are simply added together in the calculation, the uniform source angle distribution gives the fastest decay rate of the non-physical fluctuation as a function of source number (faster than N^{-10}). With the same source number, the random distribution gives much poorer Green's function reconstruction. The rate of the non-physical fluctuation decay is approximately N^{-1}. The distribution with the source angle smoothly varying behaves closer to the uniform distribution than random distribution.

For interferometry for the diffusion equation in a homogeneous medium, a finite number of source suffices to reconstruct the Green's function. For a 1-D model, the sensitivity of the sources decays away from the center of the two receivers. The width of the distribution controls the late-time of the reconstructed Green's function while the source density controls the early-time of the reconstructed Green's function. For a 3-D model, the main properties are the same as the 1-D problem. What special in 3-D problem is that the two receiver positions are the two singularities in the calculation. Consequently, the source should not be too close to the receiver positions. Otherwise, the contribution from that source is over weighted and the reconstruction becomes not accurate. Different from the cross-correlation-based interferometry, the deconvolution-based interferometry shows special properties for the diffusion equation. For 3-D diffusion problem in a homogeneous medium, one source is enough to reconstruct accurate Green's function if deconvolution is used in the calculation.

REFERENCES

Bakulin, Andrey, & Calvert, Rodney. 2004. Virtual source: new method for imaging and 4D below complex overburden. *SEG Technical Program Expanded Abstracts*, **23**, 2477–2480.

Bakulin, Andrey, & Calvert, Rodney. 2006. The virtual source method: Theory and case study. *Geophysics*, **71**, SI139–SI150.

Calvert, R.W., Bakulin, A., & Joners, T.C. 2004. Virtual Sources, a new way to remove overburden problems. *Expanded abstracts of the 2004 EAEG-meeting*, 2477–2480.

Campillo, Michel, & Paul, Anne. 2003. Long-Range Correlations in the Diffuse Seismic Coda. *Science*, **299**, 547–549.

Constable, S., & Srnka, L. J. 2007. An introduction to marine controlled-source electromagnetic methods for hydrocarbon exporation. *Geophysics*, **72**, WA3–WA12.

Curtis, Andrew, Gerstoft, Peter, Sato, Haruo, Snieder, Roel, & Wapenaar, Kees. 2006. Seismic interferometry-turning noise into signal. *The Leading Edge*, **25**, 1082–1092.

Darnet, M., Choo, M. C. K., Plessix, R. E., rosenquist, M. L., Yip-Cheong, K., Sims, E., & Voon, J. W. K. 2007. Detecting hydrocarbon reservoirs from CSEM data in complex setting: Application to deepwater Sabah, Malaysia. *Geophysics*, **72**, WA97–WA103.

Derode, Arnaud, Larose, Eric, Campillo, Michel, & Fink, Mathias. 2003. How to estimate the Green's function of a heterogeneous medium between two passive sensors? Application to acoustic waves. *Appl. Phys. Lett.*, **83**, 3054–3056.

Godin, Oleg A. 2006. Recovering the Acoustic Green's Function from Ambient Noise Cross Correlation in an Inhomogeneous Moving Medium. *Phys. Rev. Lett.*, **97**, 054301–4.

Groenenboom, J., & Snieder, R. 1995. Attenuation, Dispersion and Anisotropy by Multiple Scattering of Transmitted Waves Through Distributions of Scatterers. *J. Acoust. Soc. Am.*, **98**, 3482–3492.

Hoversten, G. M., Newman, G. A., Geier, N., & Flanagan, G. 2006. 3D modeling of a deepwater EM exploration survey. *Geophysics*, **71**, G239–G248.

Larose, Eric, Montaldo, Gabriel, Derode, Arnaud, & Campillo, Michel. 2006. Passive imaging of localized reflectors and interfaces in open media. *Appl. Phys. Lett.*, **88**, 104103.

Lobkis, Oleg I., & Weaver, Richard L. 2001. On the emergence of the Green's function in the correlations of a diffuse field. *J. Acoust. Soc. Am.*, **110**, 3011–3017.

Malcolm, Alison E., Scales, John A., & van Tiggelen, Bart A. 2004. Extracting the Green function from diffuse, equipartitioned waves. *Phys. Rev. E.*, **70**, 015601.

Mehta, K., Bakulin, A., Sheiman, J., Calvert, R., & Snieder, R. 2007a. Improving the virtual source method by wavefield separation. *Geophysics*, **72**, V79–V86.

Mehta, Kurang, Snieder, Roel, & Graizer, Vladimir. 2007b. Downhole Receiver Function: a Case Study. *Bull. Seismol. Soc. Am.*, **97**, 1396–1403.

Nokken, M. R., & Hooton, R. D. 2007. Using pore parameters to estimate permeability or conductivity of concrete. *Materials and Structures*, **41**, 1–16.

Rickett, J., & Claerbout, J. 1999. Acoustic daylight imaging via spectral factorization: Helioseismology and reservoir monitoring. *The Leading Edge*, 957–960.

Roux, Philippe, Sabra, Karim G., Kuperman, W. A., &

Roux, Andre. 2005. Ambient noise cross correlation in free space: Theoretical approach. *J. Acoust. Soc. Am.*, **117**, 79–84.

Sabra, Karim G., Gerstoft, Peter, Roux, Philippe, Kuperman, W. A., & Fehler, Michael C. 2005a. Extracting time-domain Green's function estimates from ambient seismic noise. *Geophys. Res. Lett.*, **32**, L03310.

Sabra, Karim G., Gerstoft, Peter, Roux, Philippe, Kuperman, W. A., & Fehler, Michael C. 2005b. Surface wave tomography from microseisms in Southern California. *Geophys. Res. Lett.*, **32**, L14311.

Sánchez-Sesma, F.J., & Campillo, M. 2006. Retrieval of the Green's funciton from cross correlation: The canonical elastic problem. *Bull. Seismol. Soc. Am.*, **96**, 1182–1191.

Sánchez-Sesma, F.J., Pérez-Ruiz, J.A., Campillo, M., & Luzón, F. 2006. Elastodynamic 2D Green function retrieval from cross-correlation: Canonical inclusion problem. *Geophys. Res. Lett.*, **33**, L13305, doi:10.1029/2006GL026454.

Scholl, C., & Edwards, R. N. 2007. Marine downhole to seafloor dipole-dipole electromagnetic methods and the resolution of resistive targets. *Geophysics*, **72**, WA39–WA49.

Schuster, G. T., Yu, J., Sheng, J., & Rickett, J. 2004. Interferometric/daylight seismic imaging. *Geophys. J. Int.*, **157**, 838–852.

Shapiro, Nikolai M., Campillo, Michel, Stehly, Laurent, & Ritzwoller, Michael H. 2005. High-Resolution Surface-Wave Tomography from Ambient Seismic Noise. *Science*, **307**, 1615–1618.

Snieder, Roel. 2004. Extracting the Green's function from the correlation of coda waves: A derivation based on stationary phase. *Phys. Rev. E*, **69**, 046610.

Snieder, Roel. 2006a. *A Guided Tour of Mathematical Methods: For the Physical Sciences*. 2 edn. Cambridge University Press.

Snieder, Roel. 2006b. Retrieving the Green's function of the diffusion equation from the response to a random forcing. *Phys. Rev. E*, **74**, 046620.

Snieder, Roel. 2007. Extracting the Green's function of attenuating heterogeneous acoustic media from uncorrelated waves. *J. Acoust. Soc. Am.*, **121**, 2537–2643.

Snieder, Roel, & Safak, Erdal. 2006. Extracting the Building Response Using Seismic Interferometry: Theory and Application to the Millikan Library in Pasadena, California. *Bull. Seismol. Soc. Am.*, **96**, 586–598.

Snieder, Roel, Sheiman, Jon, & Calvert, Rodney. 2006. Equivalence of the virtual-source method and wave-field deconvolution in seismic interferometry. *Phys. Rev. E*, **73**, 066620.

Snieder, Roel, Wapenaar, Kees, & Wegler, Ulrich. 2007. Unified Greens function retrieval by cross-correlation; connection with energy principles. *Phys. Rev. E.*, **75**, 036103.

Stehly, L., Campillo, M., & Shapiro, N. M. 2006. A study of seismic noise from its long-range correlation properties. *J. Geophys. Res.*, **111**, B10306.

Trampert, J., Cara, M., & Frogneux, M. 1993. *SH* propagator matrix and Q_s estimates from borehole- and surface-recorded earthquake data. *Geophys. J. Int.*, **112**, 290–299.

van Manen, Dirk-Jan, Robertsson, Johan O. A., & Curtis, Andrew. 2005. Modeling of Wave Propagation in Inhomogeneous Media. *Phys. Rev. Lett.*, **94**, 164301.

van Wijk, K. 2006. On estimating the impulse response between receivers in a controlled ultrasonic experiment. *Geophysics*, **71**, SI79–SI84.

Vasconcelos, Ivan, & Snieder, Roel. 2006. Interferometric imaging by deconvolution: Theory and numerical examples. *SEG Technical Program Expanded Abstracts*, **25**, 2416.

Vasconcelos, Ivan, Snieder, Roel, & Hornby, Brian. 2007. Target-oriented interferometry — Imaging with internal multiples from subsalt VSP data. *SEG Technical Program Expanded Abstracts*, **26**, 3069–3073.

Voyiadjis, George Z., & Song, Chung R. 2003. Determination of Hydraulic Conductivity Using Piezocone Penetration Test. *Int. J. Geomech.*, **3**, 217–224.

Wapenaar, Kees. 2004. Retrieving the Elastodynamic Green's Function of an Arbitrary Inhomogeneous Medium by Cross Correlation. *Phys. Rev. Lett.*, **93**, 254301–4.

Wapenaar, Kees. 2006a. Green's function retrieval by cross-correlation in case of one-sided illumination. *Geophys. Res. Lett.*, **33**, L19304.

Wapenaar, Kees. 2006b. Non-reciprocal Green's function retrieval by cross correlation. *J. Acoust. Soc. Am.*, **120**, EL7–EL13.

Wapenaar, Kees, Fokkema, Jacob, & Snieder, Roel. 2005. Retrieving the Green's function in an open system by cross-correlation : a comparison of approaches. *J. Acoustic. Soc. Am.*, **118**, 2783–2786.

Wapenaar, Kees, Slob, Evert, & Snieder, Roel. 2006. Unified Green's Function Retrieval by Cross Correlation. *Phys. Rev. Lett.*, **97**, 234301.

Weaver, Richard L. 2005. Information from seismic noise. *Science*, **307**, 1568–1569.

Weaver, Richard L., & Lobkis, Oleg I. 2001. Ultrasonics without a Source: Thermal Fluctuation Correlations at MHz Frequencies. *Phys. Rev. Lett.*, **87**, 134301.

Weaver, Richard L., & Lobkis, Oleg I. 2004. Diffuse fields in open systems and the emergence of the Green's function (L). *J. Acoust. Soc. Am.*, **116**, 2731–2734.

Weaver, Richard L., & Lobkis, Oleg I. 2005. Fluctuations in diffuse field–field correlations and the emergence of the Green's function in open systems. *J. Acoust. Soc. Am.*, **117**, 3432–3439.

Weaver, R.L. 2008. Ward identities and he retrieval of Green's functions in the corre- lations of a diffuse field. *Wave Motion, in press.*